European Journal of Radiology 171 (2024) 111282

Contents lists available at ScienceDirect

European Journal of Radiology

journal homepage: www.elsevier.com/locate/ejrad

Research article

Image quality assessment of coronary artery segments using ultra-high resolution dual source photon-counting detector computed tomography

Judith van der Bie [a,1], Simran P. Sharma [a,b,1], Marcel van Straten [a], Alexander Hirsch [a,b], Putri Annisa Kamila [a], Daniel Bos [a,c], Marcel L. Dijkshoorn [a], Ronald Booij [a], Ricardo P.J. Budde [a,b,*]

[a] Department of Radiology & Nuclear Medicine, Erasmus MC, University Medical Center Rotterdam, Rotterdam, the Netherlands
[b] Department of Cardiology, Erasmus MC, University Medical Center Rotterdam, Rotterdam, the Netherlands
[c] Department of Epidemiology, Erasmus MC, University Medical Center Rotterdam, Rotterdam, the Netherlands

ARTICLE INFO

Keywords:
Coronary computed tomography angiography
Photon-counting detector CT
Ultra-high resolution
Coronary artery disease
Image quality

ABSTRACT

Purpose: The study is intended to assess the image quality of ultra-high resolution (UHR) coronary computed tomography angiography (CCTA) performed on dual source photon-counting detector CT (PCD-CT).
Method: Consecutive patients, who underwent clinically indicated CCTA on PCD-CT (UHR 120x 0.2 mm collimation), were included. CCTA images were reconstructed at 0.2 mm slice thickness with Bv40, Bv44, Bv48 and Bv56 kernels and quantum iterative reconstruction level 4. Contrast-to-noise (CNR) and signal-to-noise ratios (SNR) were quantified from contrast-enhanced blood and subcutaneous adipose tissue. All reconstructions were scored per coronary segment (18-segment model) for presence, image quality, motion artefacts, stack artefacts, plaque presence and composition, and stenosis degree. Image quality was scored by two independent observers.
Results: Sixty patients were included (median age 62 [25th ‾ 75th percentile: 53–67] years, 45% male, median calcium score 62 [0–217]). The mean heart rate during scanning was 71 ± 11 bpm. Median CTDIvol was 19 [16–22]mGy and median DLP 243 [198–327]mGy.cm. The SNR was 9.3 ± 2.3 and the CNR was 11.7 ± 2.6. Of the potential 1080 coronary segments (60 patients x 18 segments), 255/256 (reader1/reader2) segments could not be assessed for being absent or non-evaluable due to size. Both readers scored 85% of the segments as excellent or very good (Intraclass Correlation Coefficient: 0.88 (95% CI: 0.87–0.90). Motion artefacts were present in 45(5%) segments, stack artefacts in 60(7%) segments and metal artefacts in 9(1%) segments.
Conclusion: UHR dual-source PCD-CT CCTA provides excellent or very good image quality in 85% of coronary segments at relatively high heart rates at moderate radiation dose with only limited stack artefacts.

1. Introduction

Coronary computed tomography angiography (CCTA) is the primary non-invasive imaging modality to evaluate the presence and severity of coronary artery disease (CAD) [1]. The current energy-integrating detector (EID) technology is well established but has a limited spatial resolution. This limitation hampers its diagnostic accuracy when quantifying stenosis in small coronary arteries, especially in the presence of high-contrast objects such as calcifications and stents [2].

Photon-counting detectors (PCDs) possess the capability of measuring individual incoming X-ray photons and exhibit an improved geometric detector efficiency in comparison to EIDs (3). In ultra-high resolution (UHR) mode, PCD-CT offers a maximal spatial resolution in the Z-direction of 0.2 mm and a maximal in-plane resolution of 0.11 mm

Abbreviations: CAD, coronary artery disease; CCTA, coronary computed tomography angiography; CNR, contrast-to-noise ratio; $CTDI_{VOL}$, volume computed tomography dose index; DLP, dose length product; EID, energy-integrating detector; HU, Hounsfield Units; ICC, Intraclass Correlation Coefficient; PCD, photon-counting detector; ROI, region-of-interest; SNR, signal-to-noise ratio; UHR, ultra-high resolution.

* Corresponding author at: Department of Radiology & Nuclear Medicine, Erasmus MC, University Medical Center Rotterdam, Rotterdam, the Netherlands.
E-mail addresses: j.vanderbie@erasmusmc.nl (J. van der Bie), s.sharma@erasmusmc.nl (S.P. Sharma), marcel.vanstraten@erasmusmc.nl (M. van Straten), a.hirsch@erasmusmc.nl (A. Hirsch), p.kamila@erasmusmc.nl (P.A. Kamila), d.bos@erasmusmc.nl (D. Bos), m.l.dijkshoorn@erasmusmc.nl (M.L. Dijkshoorn), r.booij@erasmusmc.nl (R. Booij), r.budde@erasmusmc.nl (R.P.J. Budde).
[1] These authors have contributed equally and share first authorship.

https://doi.org/10.1016/j.ejrad.2023.111282
Received 4 August 2023; Received in revised form 21 November 2023; Accepted 28 December 2023
Available online 3 January 2024

[3,4]. This represents a threefold improvement in z-axis resolution over conventional CT (0.6 mm) and may lead to the sharper depiction of coronary arteries, decreased partial volume effect, and reduced blooming artefact of high attenuating objects such as coronary calcifications, mechanic valves, and stents [5,6]. These factors can collectively contribute to the enhanced utility of PCD-CT over conventional EID-CT in clinical settings.

Initial feasibility studies, performed with PCD-CTs from different vendors, showed improved stent assessment, image quality, diagnostic confidence and reduced calcium blooming for UHR PCD-CT for CCTA [3,7,8] in a very limited number of patients. In the present study, we aimed to evaluate the image quality of UHR PCD-CT for CCTA in a larger sample size of consecutive patients, in routine clinical practice on a clinical photon-counting system and assessed image quality per coronary segment.

2. Methods

2.1. Patient inclusion

For the current study, we included 60 consecutive patients who underwent UHR CCTA on a dual-source PCD-CT (Siemens NAEOTOM Alpha, Siemens Healthineers VA50) as part of routine clinical care between May 2022 and January 2023. Exclusion criteria encompassed patients who were not scanned in UHR mode and those unable to provide informed consent. This study was performed in line with the principles of the Declaration of Helsinki and all patients signed informed consent for use of their data. Full review and approval were waived by the ethics committee because of the observational, retrospective nature of the study. Data on the patient characteristics (demographics, cardiac history including percutaneous coronary intervention with stent placement, coronary artery bypass graft, pacemaker or implantable cardioverter-defibrillator implantation, heart transplantation or valve replacement), coronary artery calcium scores, CCTA indications and radiation dose, were obtained from electronic health records.

2.2. Image acquisition and reconstruction

First, a non-contrast acquisition was performed to determine the patient's coronary artery calcification scores (120 kV, image quality level 16). Subsequently, a CCTA of the heart was performed with prospective ECG-triggering, a tube voltage of 120 kV or 140 kV (chosen by the technicians based on the best fit for the patient and taking into account the maximum tube current limit), collimation of 120 x 0.2 mm and 0.25 s rotation time. For patients with a stable sinus rhythm and a heart rate of ≤75 beats per minute (bpm), the ECG-pulsing window was set to 35% to 60% of the R-R interval. For patients with a heart rate of >75 bpm the ECG-pulsing window was set to 67% to 83% of the R-R interval. In case of atrial fibrillation or arrhythmia, retrospective gating or wide padding was used. Image quality level was set to 65, the tube current was automatically adjusted to achieve this image quality level. However, in some cases the maximum tube current was reached, and the image quality level was automatically lowered. CCTA images were reconstructed using a slice thickness of 0.2 mm and 0.15 mm increments, with four different reconstruction kernels (Bv40, Bv44, Bv48, Bv56) on Quantum Iterative Reconstruction (QIR) strength 4. Reconstructed matrix size (512 x 512 pixels, 768 x 768 pixels or 1024 x 1024 pixels) was automatically determined by the scanner such that the pixel size does not negatively affect the image resolution.

For the contrast injection protocol, a test bolus of 15 mL was administered, followed by a saline flush of 10 mL. Subsequently, a standard amount of 85 mL of iodinated contrast medium (Visipaque 320 mg iodine/mL (Jodixanol), GE Healthcare) was delivered, followed by a saline chaser (NaCl 0.9 %) of 40 mL. The flow rate for all was 5 mL/s.

Patients were administered beta-blockers as indicated on the request form or when the heart rate exceeded 90 bpm. Nitroglycerin was administered only when specified on the request form and in the absence of contraindications.

2.3. Assessment of image quality

For the quantitative analysis, images with the sharpest kernel (Bv56, QIR = 4) available were used to place a region-of-interest (ROI) in the ascending aorta and subcutaneous adipose tissue (sat). ROIs were drawn as large as possible to determine mean CT numbers, expressed in Hounsfield Units (HU), and standard deviations (STD). From these values, signal-to-noise ratio (SNR) and contrast-to-noise ratio (CNR) were derived by the following equations:

$$SNR = \frac{MEAN_{aorta}}{STD_{aorta}} \quad (1)$$

and

$$CNR = \frac{MEAN_{aorta} - MEAN_{sat}}{STD_{aorta}} \quad (2)$$

For the qualitative analysis, one radiologist (RJPB) with > 15 years of experience in cardiovascular CT and one cardiologist (PAC) with > 3 years of experience in cardiovascular CT assessed each UHR scan per coronary segment using the 18-segment model of the Society of Cardiovascular Computed Tomography [9]. The observers used the best available highest kernel (Bv56) in this study or switched to a lower one in case of too noisy images. First, the segments were scored as present, absent, non-evaluable due to size or image quality. A segment was scored as absent when that coronary segment was not visible despite image quality deemed sufficient to say that had the segment been present it would have been seen. Absent segments were not included in further analysis. Both observers assessed the overall quality of the coronary segments and the cardiac structures, including the aortic valve, mitral valve, and left ventricle. The overall quality was graded using a 5-point Likert scale (Fig. 1). In addition, the radiologist visually scored each segment for the presence of stents, motion artefacts, stack artefacts, other (metal/stent) artefacts, presence of plaque (yes/no), plaque composition (calcified, non-calcified, mixed) and degree of diameter stenosis (0%, 1–24%, 25–49%, 50–69%, 70–89%, ≥90%, non-evaluable). The stenosis degree was scored by "eye-balling". For the analysis of image quality and segment size, we stratified the coronary segments into proximal and mid/distal segments. The proximal segments included: the proximal right coronary artery, left main artery, proximal left anterior descending artery, and proximal left circumflex artery. The mid/distal segments included: mid right coronary artery, distal right coronary artery, right posterior descending artery, right posterolateral branch, mid left anterior descending artery, distal left anterior descending artery, mid and distal left circumflex artery, left posterior descending artery, and left posterolateral branch. We excluded side branches including diagonal branches, obtuse marginal branches, and the intermediate branch from the analysis.

2.4. Statistical analysis

Categorical variables are expressed as frequencies and percentages, continuous variables were expressed as mean ± standard deviation or as median with [25th − 75th percentile], depending on the distribution. Shapiro-Wilk test was used to assess the assumption of normal distribution. Inter-rater reliability was assessed using a two-way mixed-effects model Intraclass Correlation Coefficient (ICC) analysis. For the analysis of image quality and segment sizes, a linear-by-linear association Chi-Square test was conducted. All statistical analyses were performed using SPSS statistical software (IBM Corp. Released 2016. IBM SPSS Statistics for Windows, Version 28.0.1.0 Armonk; NY: IBM Corp.) and Python (Python Software Foundation. Python Language Reference, version 3.9).

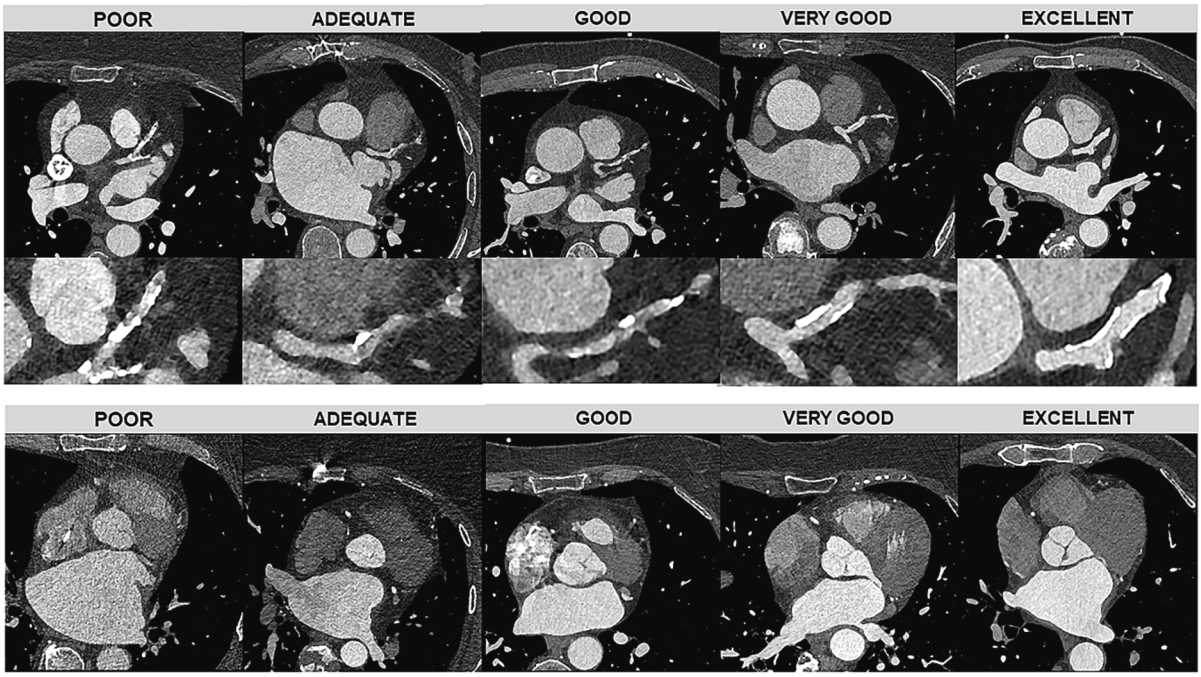

Fig. 1. Subjective image scoring method. Illustrative examples of the 5-point Likert scale measure image quality scores. The upper image shows: 1–Poor (severe artefacts/noise or insufficient vessel opacification), 2–adequate (interpretable, moderate artefacts/noise), 3-good (moderate artefacts, good opacification), 4-very good (mild artefacts, superior opacification) and 5–excellent for mid left anterior descending artery. The lower images demonstrate image quality for the aortic valve.

3. Results

3.1. Study population

A total of 60 patients (median age 62 [25th ‾ 75th percentile: 53–67] years; 27 (45%) men) were included. The indication for scanning was the evaluation of CAD (n = 39), post-heart transplantation follow-up (n = 20) and pulmonary vein ablation planning (n = 1). Six (10%) patients had one or multiple coronary stents implanted, 6 (10%) patients had a pacemaker implantation, and 2 (3%) patients had a valve replacement. The mean heart rate during scanning was 71 ± 11 bpm. The number of z-axis image stacks used was 5 (n = 10), 6 (n = 34), 7 (n = 10) or 8 (n = 6). Median $CTDI_{VOL}$ for the CCTA scans was 19 [16–22] mGy and median DLP was 243 [198–327] mGy.cm, corresponding to median effective doses of 3.4 [2.8–4.6] mSv. The patient characteristics and the radiation dose are presented in Table 1.

3.2. Objective assessment

The overall SNR was 9.3 ± 2.3 and CNR was 11.7 ± 2.6 with an average noise of 47.9 ± 10.3 HU. Eleven patients were scanned with 140 kV. The SNR (8.9 ± 2.8 vs 9.4 ± 2.2, p = 0.51) and CNR (11.6 ± 3.3 vs 11.7 ± 2.5, p = 0.89) were similar for patients scanned at 140 kV and 120 kV.

3.3. Subjective assessment

Of the potential 1080 coronary segments (60 patients x 18 segments), reader 1 scored 218 (20%) as absent, 37 (3%) as non-evaluable due to size and 10 (1%) as non-evaluable due to quality. Reader 2 scored 216 (20%) as absent, 40 (4%) as non-evaluable due to size and 8 (1%) as non-evaluable due to quality. The subjective assessment, including all segments evaluated by both readers, demonstrated that 94% of the evaluated segments were rated at least good, and 85% as very good or excellent. Reader 1 scored 698/825 (85%) as very good or excellent and reader 2 scored 701/824 (85%) as very good or excellent. The ICC between the two readers for the per segment image quality was found to be 0.88 (95 % CI: 0.87–0.90), indicating strong agreement. Detailed scores are presented in Table 2 and Fig. 2. Fig. 3 showcases extensive calcification alongside excellent image quality of the coronary segments.

Table 1
Baseline study characteristics.

Patient characteristics	N = 60
Male (%)	27 (45)
Age (years)	62 [53–67]
Body mass index (kg/m^2)	25 [23–28]
History of PCI with stent placement (%)	6 (10)
Coronary artery bypass grafting (%)	0 (0)
Valve surgery (%)	2 (3)
Pacemaker implantation (%)	6 (10)
Heart rate (beats per minute)	71 (±11)
Median calcium score	62 [0–217]*
Indications	
Coronary artery disease (%)	39 (65)
Post heart transplant (%)	20 (33)
Pulmonary vein anatomy pre ablation (%)	1 (2)
CCTA Radiation dose	
DLP (mGy.cm)	243 [198–327]
$CTDI_{vol}$ (mGy)	19 [16–22]

Data is presented as mean ± Standard Deviation (SD), median [25th – 75th percentile] , or frequencies (percentage). Coronary computed tomography angiography (CCTA); Percutaneous Coronary Intervention (PCI); Volumetric computed tomography dose index ($CTDI_{vol}$) *Calcium scores of 54 patients. No calcium score was calculated for patients (n = 6) with PCI due to stents artefacts

Table 2
Image quality per coronary segment.

Image quality score	Reader 1 (n = 825)	Reader 2 (n = 824)
1 - poor	16 (2 %)	12 (1 %)
2 - adequate	23 (3 %)	23 (3 %)
3 - good	78 (9 %)	80 (10 %)
4 - very good	180 (22 %)	195 (24 %)
5 - excellent	518 (63 %)	506 (61 %)
Non-evaluable due to quality	10 (1 %)	8 (1 %)

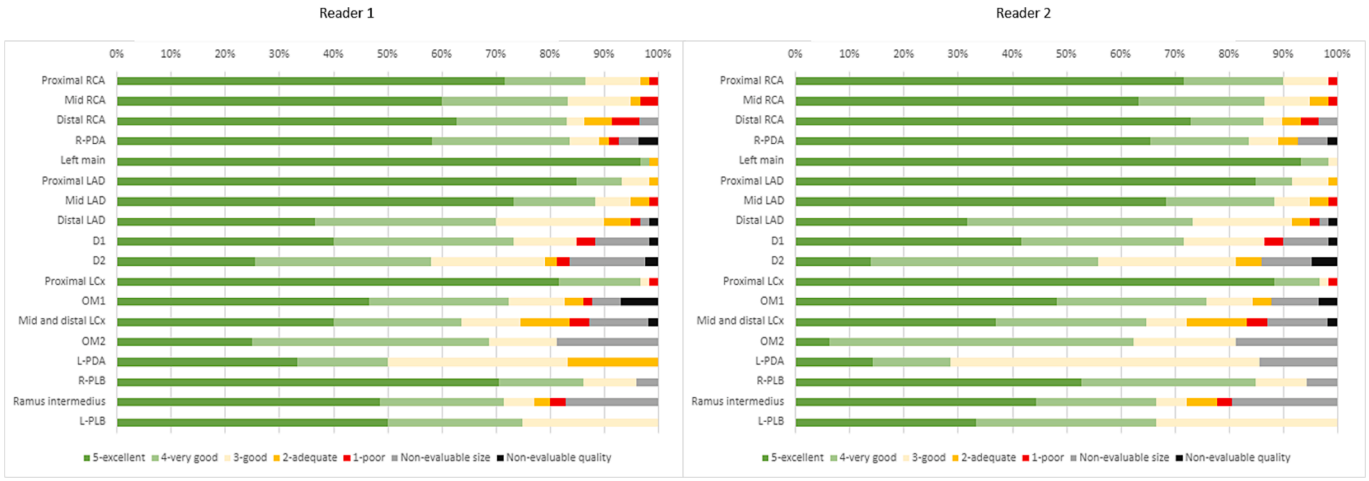

Fig. 2. Subjective assessment of the coronary segments. *The x-axis represents the percentage of coronary segments, ranging from 0% to 100%. The y-axis represents the 18 different coronary segments. Each segment is divided into coloured sections, with the size of each section corresponding to the percentage of that segment with a particular quality score. The colour of each section represents the corresponding quality score (graded using the 5-point Likert scale). Proximal RCA = Proximal Right Coronary Artery; Mid RCA = Mid Right Coronary Artery; Distal RCA = Distal Right Coronary Artery; R-PDA = Right Posterior Descending Artery; Left main = Left Main Coronary Artery; Proximal LAD = Proximal Left Anterior Descending Artery; Mid LAD = Mid Left Anterior Descending Artery; Distal LAD = Distal Left Anterior Descending Artery; D1 = First Diagonal Branch of the LAD; D2 = Second Diagonal Branch of the LAD; Proximal LCx = Proximal Left Circumflex Artery; OM1 = First Obtuse Marginal Branch of the LCx; Mid and distal LCx = Mid and Distal Left Circumflex Artery; OM2 = Second Obtuse Marginal Branch of the LCx; L-PDA = Left Posterior Descending Artery; R-PLB = Right Posterolateral Branch; Ramus intermedius = Ramus Intermedius; L-PLB = Left Posterolateral Branch.*

Motion artefacts were observed in 45 (5%) segments and stack artefacts in 60 segments (7%). Of the 13 patients with metallic implants (pacemakers, prosthetic heart valves or coronary stents), the image quality of 9 (5%) segments of the 179 present segments (13 patients x 18 segments = 234 potential segments) was impacted by metal artefacts.

Reader 1 scored 16 segments as poor in 9 patients, whereas reader 2 scored 12 segments as poor in 7 patients. The average heart rate of all patients was 71 bpm and the average heart rate of patients with segments scored as poor was 74 bpm (reader 1) and 75 bpm (reader 2). The median body mass index for all patients was 25 [23–28] versus 26 [23–28] for patients with segments scored as poor. (Sup. Tables S1 and 2). Of the segments scored as poor by reader one, 8/16 (50%) exhibited stack artefacts, 5/16 (31%) displayed motion artefacts, 1/12 (6%) manifested other artefacts, and 11/16 (73%) featured calcifications (Sup. Table S3). The median image quality score was consistently 5 across different coronary calcium score categories (Sup. Table S4).

The overall image quality scores of the aortic valve, mitral valve and left ventricle for reader 1 were at least good in 93%, 90% and 95%, respectively. Reader 2 scored these cardiac structures as at least good in 97%, 93% and 98%. Detailed scores are presented in Table 3. In addition, Fig. 4 shows examples of determinants impacting image quality.

Six patients had one or more coronary stents: 2 patients had stents in the left main artery, 3 patients in the proximal left anterior descending artery, 3 patients in the mid left anterior descending artery, 1 patient in the distal left anterior descending artery, 1 patient in the proximal left circumflex, 1 patient in the distal left circumflex artery and 1 patient in the posterior-lateral branch of the right coronary artery. For all 6 proximal segments, reader 1 graded them as excellent (100%), while reader 2 graded 5 of them (84%) as excellent. In the mid and distal segments, reader 1 evaluated 2 segments (33%) as good, while reader 2 assessed 1 segment (17%) as good. Both readers rated 1 segment (17%) as very good, and reader 1 graded 3 segments (50%) as excellent, while reader 2 rated 4 segments (67%) as excellent. Fig. 5 showcases in-vivo stents.

Table 4 presents an analysis of image quality and segment size, stratified into proximal and mid/distal coronary segments. We analysed 480 proximal segments and 785 mid/distal segments. Proximal segments exhibited a higher proportion of excellent or very good image quality scores compared to mid/distal segments. Specifically proximal segments had 84% rated as excellent and 10% as very good, while mid/distal segments had 59% rated as excellent and 25% as very good ($p < 0.001$).

In 14 out of 815 segments (825 – 10 non evaluable segments), the degree of stenosis could not be evaluated. Overall, 545 (68%) segments had no luminal narrowing (0%), 154 (19%) segments had a luminal narrowing of 1–24%, 53 (7%) of 25–49%, 33 (4%) of 50–69%, 9 (1%) of 70–98%, 4 (1%) of ≥ 90% and three (1%) segments were fully occluded. Of the 270 plaques, one was not assessable. Of the remaining 269 plaques, 221 (82%) were calcified, 6 (2%) were non-calcified and 42 (16%) were mixed plaques.

4. Discussion

This study aimed to evaluate the performance of UHR PCD-CT in assessing coronary segments. The subjective assessment demonstrated that 94% of the evaluated coronary segments were rated at least good and 85% as very good or excellent, even at relatively high heart rates and with moderate radiation doses (within the recommended diagnostic reference levels [10]), and limited stack artefacts were observed. These results indicate the potential of UHR PCD-CT to provide high-quality images for the evaluation of coronary segments.

Our results are in line with previous research. Mergen et al. reported comparable SNR and CNR values (10.4 ± 2.2 and 12.5 ± 2.6 respectively) using Bv56 QIR4 kernels in UHR PCD-CT for 20 patients. Mergen et al. also observed that using sharper kernels led to a reduction in SNR, CNR and blooming artefacts, while vessel sharpness increased. Kernels sharper than Bv72 did not show a significant improvement in blooming artefacts [3].

In our study, the degree of stenosis could not be assessed in only 2% of the segments. Koons et al. found reduced degree of coronary stenosis with PCD-CT compared to EID-CT in patients scanned on the same day on both scanners [11]. Eberhard et al. compared stenosis grade from UHR PCD-CT angiography to 3D quantitative coronary angiography and confirmed improved accuracy and reduced variability in stenosis measurement and classification of patients with extensive calcification compared to standard resolution mode [12]. Both studies indicate that improved delineation, reduced partial volume effects, and mitigated blooming artefacts contribute to this enhancement in stenosis

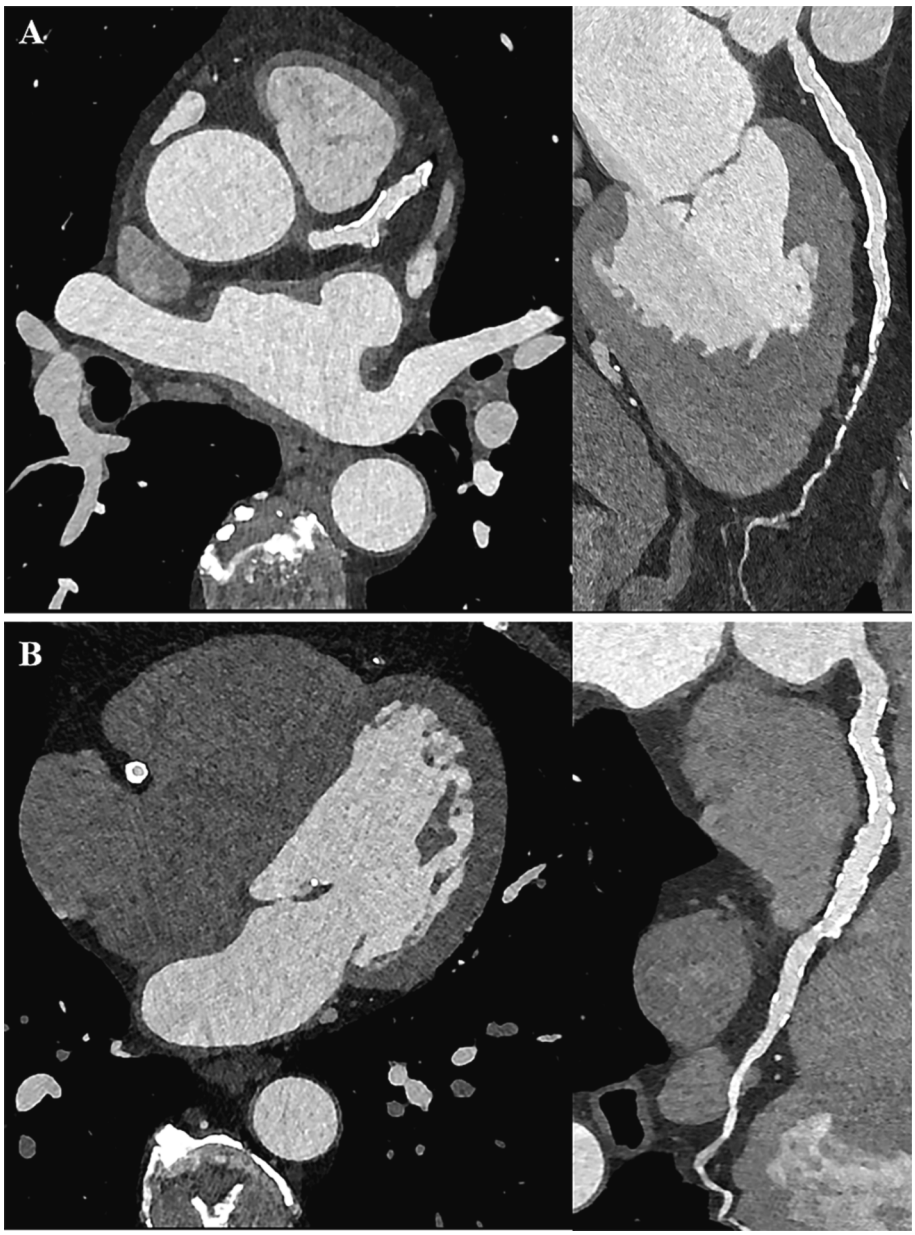

Fig. 3. Patient case with extensively calcified coronary vessel walls. *Patient scanned at 140 kV with a $CTDI_{VOL}$ of 31 mGy, with a heart rate of 64 bpm and 7 stacks). A. Extensive calcified vessel wall of the left anterior descending artery with significant lumen tapering in the mid left anterior descending artery with suspected significant stenosis scores as excellent. B. Right coronary artery with extensive circular calcifications of the vessel wall scored as excellent.*

Table 3
Image quality of the aortic valve, mitral valve and left ventricle.

Image quality score	Reader 1			Reader 2		
	Aortic valve, n (%)	Mitral valve n (%)	Left ventricle, n (%)	Aortic valve, n (%)	Mitral valve, n (%)	Left ventricle, n (%)
1 - poor	1 (2)	1 (2)	1 (2)	0 (0)	0 (0)	0 (0)
2 - adequate	3 (5)	5 (8)	2 (3)	2 (3)	4 (7)	1 (2)
3 - good	9 (15)	10 (17)	12 (20)	9 (15)	6 (10)	6 (10)
4 - very good	21 (35)	21 (35)	16 (27)	10 (17)	14 (23)	14 (23)
5 - excellent	26 (43)	23 (38)	28 (47)	39 (65)	36 (60)	39 (65)

assessment. The use of UHR mode compared to conventional CCTA, may improve the accurate identification of patients without significant stenosis, potentially increasing the specificity of CCTA and facilitating the avoidance of unnecessary additional testing, thereby reducing costs and potential harm to patients from invasive procedures [13,14].

Six patients with one or more coronary stents were included, predominately placed in the left main or proximal left anterior descending artery. Ninety-two percent of the segments with a stent were scored as excellent. These findings, along with previous studies by Boccalini et al. and Geering et al., suggest that UHR PCD-CT can play an essential role in

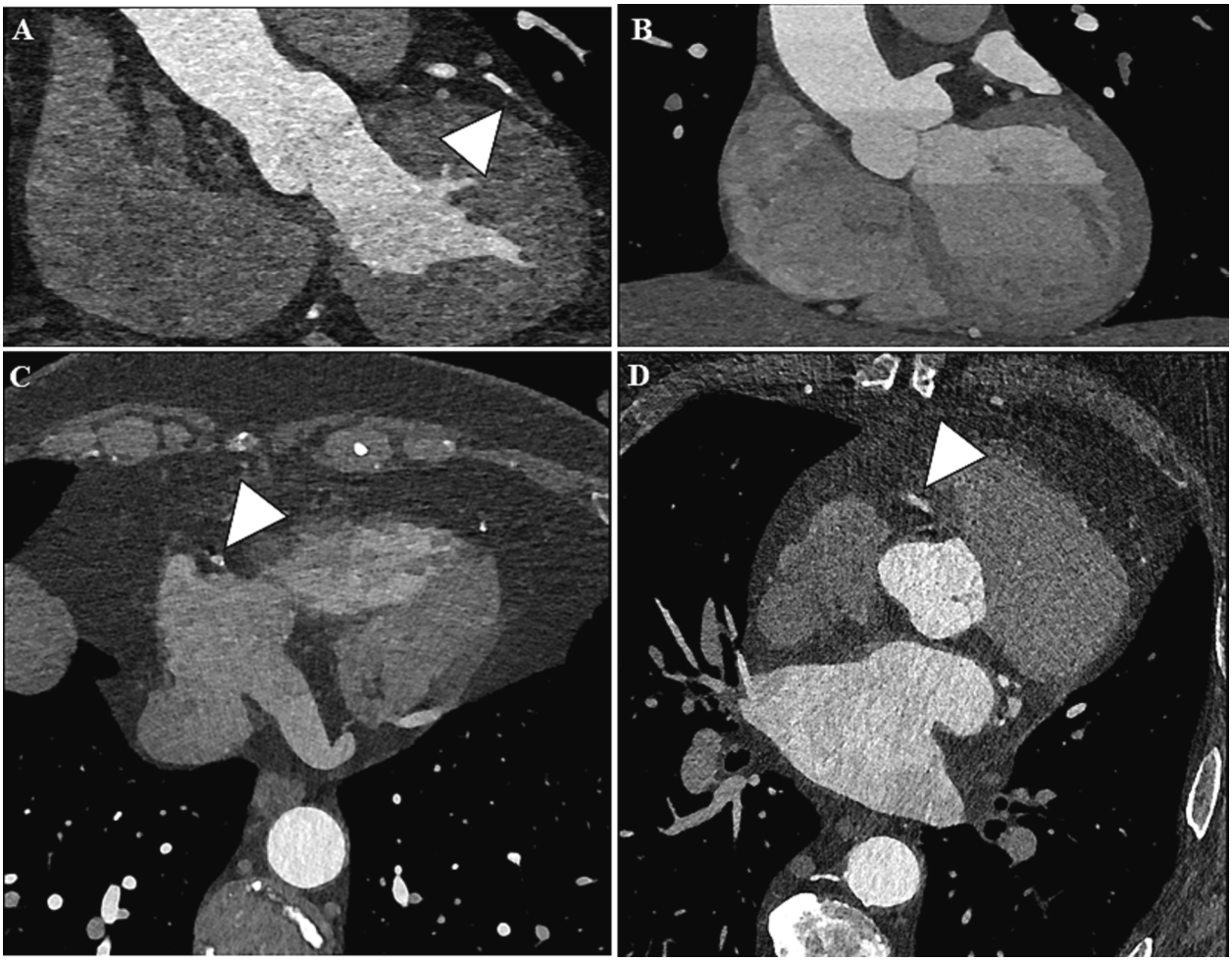

Fig. 4. Examples of factors affecting image quality. *A. Patient (male, $CTDI_{VOL}$ = 18.1 mGy) with stack artefact at the height of the second diagonal. The arrow indicates the transition of high attenuation of iodine and low attenuation in the lumen of the coronary artery. A total of 5 stacks were used with an average heart rate of 78 bpm. B. Example of a too short contrast bolus resulting in lower contrast in the caudal parts of the CTA ($CTDI_{VOL}$ = 18.9 mGy, HR = 60bmp, Stacks 6). C/D Motion artefact of the right coronary artery.*

the evaluation of coronary stents and in-stent restenosis [8,15]. Hagar et al. showed promising results for the detection of coronary stenosis in patients with 15 stents with a sensitivity of 100% (eight of eight), specificity of 86% (six of seven), and accuracy of 93% (14 of 15)[14]. To fully confirm these potential benefits, further research with bigger sample sizes are needed to investigate UHR PCD-CT its diagnostic accuracy.

Precise plaque characterization is crucial in CAD since it informs treatment decisions, guiding optimal medical therapy to prevent plaque progression and promote stabilization [16–18]. The potential of UHR PCD-CT for accurate plaque composition assessment has significant implications for clinical management and outcomes [19]. The recent study of Mergen et al. highlighted that using a sharp vessel kernel (Bv64) resulted in smaller calcified and larger non-calcified components compared to reference standard reconstructions, indicative of reduced blooming artifacts and improved visualization of non-calcified plaque components.[20] Nevertheless, further research is required to validate UHR PCD-CT's accuracy in plaque characterization with an intracoronary imaging technique as a feasible reference standard [21,22].

Next to the advantages, UHR PCD-CT comes with some challenges. The shorter z-coverage in UHR mode of 2.4 cm (120 x 0.2 mm) compared to high resolution mode (5.8 cm;144 x 0.4 mm) necessitates more stacks to image the entire heart (typically 6 or 7 as opposed to 3 to 4 in high resolution mode), and a longer scan time to cover the entire heart. This prolonged scanning duration increases the risk of motion and stack-related artefacts and requires a lengthier contrast bolus. However, we experienced only limited motion artefacts (5%) and stack artefacts (7%) in our study. This may be attributed to the high temporal resolution of the dual-source PCD-CT system used and the minimal impact of heart rate on image quality deterioration. [13,21,22].

There are some limitations regarding this study. No direct comparison with conventional CT was performed in this study due to retrospective study design and ethical considerations. Secondly, scans were only acquired at 120 kV or 140 kV. Recently, 70 kV and 90 kV scan modes have also become available for UHR imaging and are expected to further reduce the radiation dose. Lastly, due to the retrospective design of our study we did not reconstruct images with the Bv64 kernel, which is the optimal kernel in terms of vessel sharpness and blooming recommended by Mergen et al. However, regarding noise and inherently SNR and CNR the performance of Bv56 outperforms Bv64 [3].

In conclusion, UHR dual-source PCD-CT CCTA provides at least good image quality in 94% of coronary segments and very good or excellent image quality in 85% at relatively high heart rates at only moderate radiation dose and with only limited stack artefacts.

This research did not receive any specific grant from funding agencies in the public, commercial, or not-for-profit sectors.

Relation with Industry: Institutional support to Erasmus MC by Siemens Healthineers.

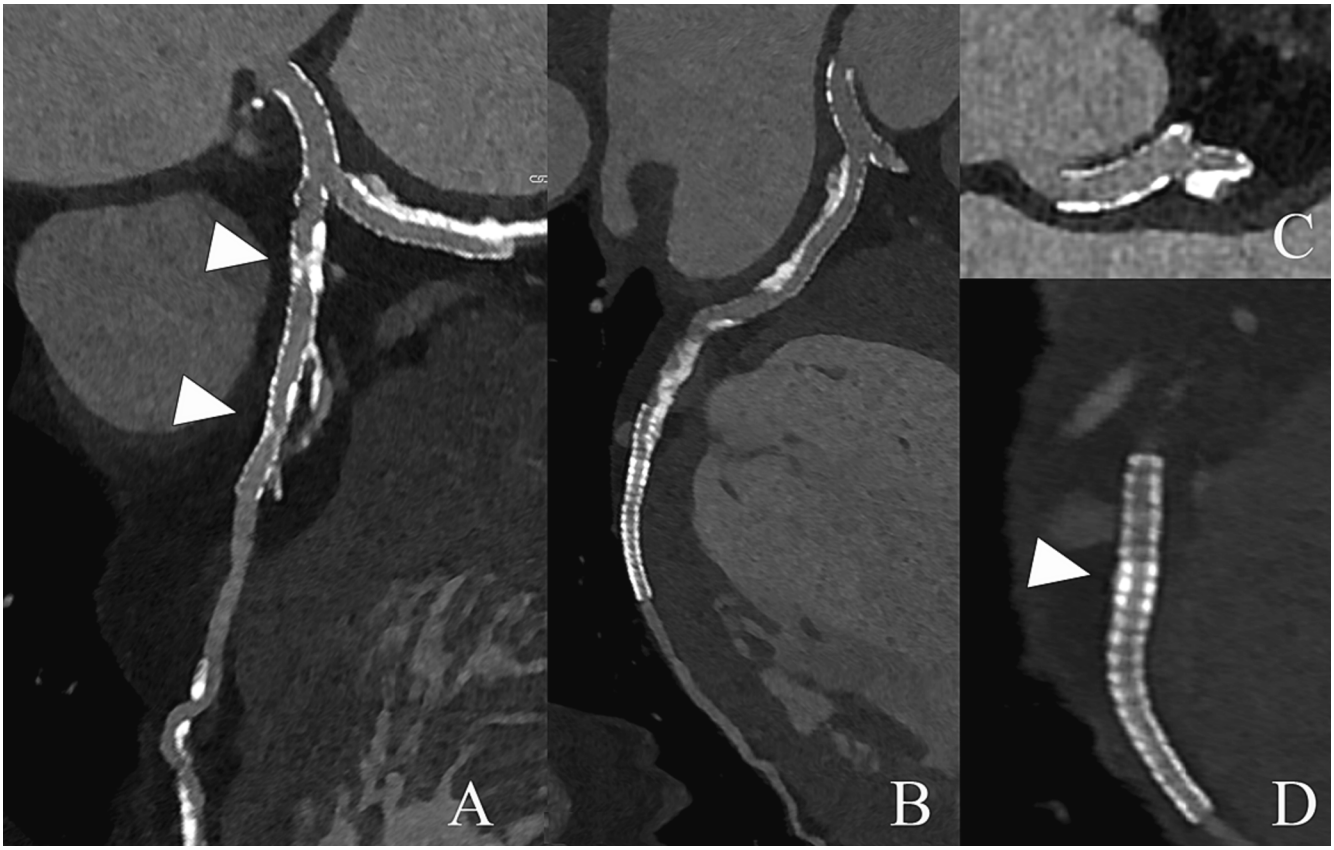

Fig. 5. Ultra high resolution CT images of a patient with multiple stents in the left main, left anterior descending and left circumflex coronary arteries.*A. Curved multiplanar reconstruction of the left anterior descending artery depicting the coronary stent with in-stent restenosis due to calcifications compression on the stent (arrowheads). B. Curved multiplanar reconstruction of the left circumflex artery (LCX) showing patent stents in the proximal and distal LCX. C. Multiplanar reconstruction depicting the patent stent in the left main. D. Zoomed in multiplanar reconstruction of the LCX showing the two overlapping stents in the distal LCX. Notice the clear depiction of the individual stent struts as well as the area where the two stents overlap (arrowheads). All reconstructions with 0.2 mm slice thickness and Bv56 kernel.*

Table 4
Image quality and segment size.

Image quality score	Proximal segments (n = 480)	Mid and distal segments (n = 785)	P value
1 - poor	4 (1)	16 (2)	<0.001
2 - adequate	4 (1)	32 (4)	
3 - good	21 (4)	81 (10)	
4 - very good	47 (10)	195 (25)	
5 - excellent	480 (84)	461 (59)	

Segments are scored independently by two readers. The numbers represent the total segments scored by both readers.

CRediT authorship contribution statement

Judith van der Bie: Writing – review & editing, Writing – original draft, Validation, Methodology, Investigation, Formal analysis, Data curation, Conceptualization. **Simran P. Sharma:** Writing – review & editing, Writing – original draft, Validation, Methodology, Investigation, Formal analysis, Data curation, Conceptualization. **Marcel van Straten:** Writing – review & editing, Supervision, Conceptualization. **Alexander Hirsch:** Writing – review & editing, Supervision, Methodology. **Putri Annisa Kamila:** . **Daniel Bos:** Writing – review & editing, Supervision, Conceptualization. **Marcel L. Dijkshoorn:** Writing – review & editing, Supervision, Conceptualization. **Ronald Booij:** Writing – review & editing. **Ricardo P.J. Budde:** .

Declaration of competing interest

The authors declare that they have no known competing financial interests or personal relationships that could have appeared to influence the work reported in this paper.

Appendix A. Supplementary data

Supplementary data to this article can be found online at https://doi.org/10.1016/j.ejrad.2023.111282.

References

[1] J. Knuuti, W. Wijns, A. Saraste, D. Capodanno, E. Barbato, C. Funck-Brentano, E. Prescott, R.F. Storey, C. Deaton, T. Cuisset, S. Agewall, K. Dickstein, T. Edvardsen, J. Escaned, B.J. Gersh, P. Svitil, M. Gilard, D. Hasdai, R. Hatala, F. Mahfoud, J. Masip, C. Muneretto, M. Valgimigli, S. Achenbach, J.J. Bax, E.S.C.S.D. Group, 2019 ESC Guidelines for the diagnosis and management of chronic coronary syndromes, Eur Heart J 41(3) (2020) 407-477.

[2] K.M. Abdelrahman, M.Y. Chen, A.K. Dey, R. Virmani, A.V. Finn, R.Y. Khamis, A. D. Choi, J.K. Min, M.C. Williams, A.J. Buckler, C.A. Taylor, C. Rogers, H. Samady, C. Antoniades, L.J. Shaw, M.J. Budoff, U. Hoffmann, R. Blankstein, J. Narula, N. N. Mehta, Coronary Computed Tomography Angiography From Clinical Uses to Emerging Technologies: JACC State-of-the-Art Review, J Am Coll Cardiol 76 (10) (2020) 1226–1243.

[3] V. Mergen, T. Sartoretti, M. Baer-Beck, B. Schmidt, M. Petersilka, J.E. Wildberger, A. Euler, M. Eberhard, H. Alkadhi, Ultra-High-Resolution Coronary CT Angiography With Photon-Counting Detector CT: Feasibility and Image Characterization, Invest Radiol 57 (12) (2022) 780–788.

[4] K. Rajendran, M. Petersilka, A. Henning, E.R. Shanblatt, B. Schmidt, T.G. Flohr, A. Ferrero, F. Baffour, F.E. Diehn, L. Yu, P. Rajiah, J.G. Fletcher, S. Leng, C. H. McCollough, First Clinical Photon-counting Detector CT System: Technical Evaluation, Radiology 303 (1) (2022) 130–138.

[5] T. Flohr, M. Petersilka, A. Henning, S. Ulzheimer, J. Ferda, B. Schmidt, Photon-counting CT review, Phys Med 79 (2020) 126–136.
[6] J.D. Schuijf, J.A.C. Lima, K.L. Boedeker, H. Takagi, R. Tanaka, K. Yoshioka, A. Arbab-Zadeh, CT imaging with ultra-high-resolution: Opportunities for cardiovascular imaging in clinical practice, J Cardiovasc Comput Tomogr 16 (5) (2022) 388–396.
[7] S.A. Si-Mohamed, S. Boccalini, H. Lacombe, A. Diaw, M. Varasteh, P.A. Rodesch, R. Dessouky, M. Villien, V. Tatard-Leitman, T. Bochaton, P. Coulon, Y. Yagil, E. Lahoud, K. Erhard, B. Riche, E. Bonnefoy, G. Rioufol, G. Finet, C. Bergerot, L. Boussel, J. Greffier, P.C. Douek, Coronary CT Angiography with Photon-counting CT: First-In-Human Results, Radiology 303 (2) (2022) 303–313.
[8] S. Boccalini, S.A. Si-Mohamed, H. Lacombe, A. Diaw, M. Varasteh, P.A. Rodesch, M. Villien, M. Sigovan, R. Dessouky, P. Coulon, Y. Yagil, E. Lahoud, K. Erhard, G. Rioufol, G. Finet, E. Bonnefoy-Cudraz, C. Bergerot, L. Boussel, P.C. Douek, First In-Human Results of Computed Tomography Angiography for Coronary Stent Assessment With a Spectral Photon Counting Computed Tomography, Invest Radiol 57 (4) (2022) 212–221.
[9] G.L. Raff, A. Abidov, S. Achenbach, D.S. Berman, L.M. Boxt, M.J. Budoff, V. Cheng, T. DeFrance, J.C. Hellinger, R.P. Karlsberg, T., Society of Cardiovascular Computed, SCCT guidelines for the interpretation and reporting of coronary computed tomographic angiography, J Cardiovasc Comput Tomogr 3 (2) (2009) 122–136.
[10] V. Tsapaki, J. Damilakis, G. Paulo, A.A. Schegerer, J. Repussard, W. Jaschke, G. Frija, CT diagnostic reference levels based on clinical indications: results of a large-scale European survey, Eur Radiol 31 (7) (2021) 4459–4469.
[11] E.K. Koons, P.S. Rajiah, J.E. Thorne, N.M. Weber, H.J. Kasten, E.R. Shanblatt, C. H. McCollough, S. Leng, Coronary artery stenosis quantification in patients with dense calcifications using ultra-high-resolution photon-counting-detector computed tomography, J Cardiovasc Comput Tomogr (2023).
[12] M. Eberhard, A. Candreva, R. Rajagopal, V. Mergen, T. Sartoretti, B.E. Stähli, C. Templin, R. Manka, H. Alkadhi, Coronary Stenosis Quantification With Ultra-High-Resolution Photon-Counting Detector CT Angiography: Comparison With 3D Quantitative Coronary Angiography, JACC Cardiovasc Imaging (2023).
[13] E. Zsarnoczay, N. Fink, U.J. Schoepf, J. O'Doherty, T. Allmendinger, J. Hagenauer, E.V. Wolf, J.P. Griffith 3rd, P. Maurovich-Horvat, A. Varga-Szemes, T. Emrich, Ultra-high resolution photon-counting coronary CT angiography improves coronary stenosis quantification over a wide range of heart rates - A dynamic phantom study, Eur J Radiol 161 (2023) 110746.
[14] M.T. Hagar, M. Soschynski, R. Saffar, A. Rau, J. Taron, J. Weiss, T. Stein, S. Faby, C. von Zur Muehlen, P. Ruile, C.L. Schlett, F. Bamberg, T. Krauss, Accuracy of Ultrahigh-Resolution Photon-counting CT for Detecting Coronary Artery Disease in a High-Risk Population, Radiology 307 (5) (2023) e223305.
[15] L. Geering, T. Sartoretti, V. Mergen, G. Cundari, S. Rusek, F. Civaia, P. Rossi, J. E. Wildberger, C. Templin, R. Manka, M. Eberhard, H. Alkadhi, First in-vivo coronary stent imaging with clinical ultra high resolution photon-counting CT, J Cardiovasc Comput Tomogr 17 (3) (2023) 233–235.
[16] S. Motoyama, H. Ito, M. Sarai, T. Kondo, H. Kawai, Y. Nagahara, H. Harigaya, S. Kan, H. Anno, H. Takahashi, H. Naruse, J. Ishii, H. Hecht, L.J. Shaw, Y. Ozaki, J. Narula, Plaque Characterization by Coronary Computed Tomography Angiography and the Likelihood of Acute Coronary Events in Mid-Term Follow-Up, J Am Coll Cardiol 66 (4) (2015) 337–346.
[17] S.B. Puchner, T. Liu, T. Mayrhofer, Q.A. Truong, H. Lee, J.L. Fleg, J.T. Nagurney, J. E. Udelson, U. Hoffmann, M. Ferencik, High-risk plaque detected on coronary CT angiography predicts acute coronary syndromes independent of significant stenosis in acute chest pain: results from the ROMICAT-II trial, J Am Coll Cardiol 64 (7) (2014) 684–692.
[18] M.C. Williams, J. Kwiecinski, M. Doris, P. McElhinney, M.S. D'Souza, S. Cadet, P.D. Adamson, A.J. Moss, S. Alam, A. Hunter, A.S.V. Shah, N.L. Mills, T. Pawade, C. Wang, J. Weir McCall, M. Bonnici-Mallia, C. Murrills, G. Roditi, E.J.R. van Beek, L. J. Shaw, E.D. Nicol, D.S. Berman, P.J. Slomka, D.E. Newby, M.R. Dweck, D. Dey, Low-Attenuation Noncalcified Plaque on Coronary Computed Tomography Angiography Predicts Myocardial Infarction: Results From the Multicenter SCOT-HEART Trial (Scottish Computed Tomography of the HEART), Circulation 141(18) (2020) 1452-1462.
[19] B. Vattay, B. Szilveszter, M. Boussoussou, M. Vecsey-Nagy, A. Lin, G. Konkoly, A. Kubovje, F. Schwarz, B. Merkely, P. Maurovich-Horvat, M.C. Williams, D. Dey, M. Kolossvary, Impact of virtual monoenergetic levels on coronary plaque volume components using photon-counting computed tomography, Eur Radiol (2023).
[20] M.C. Williams, A.J. Moss, M. Dweck, P.D. Adamson, S. Alam, A. Hunter, A.S. V. Shah, T. Pawade, J.R. Weir-McCall, G. Roditi, E.J.R. van Beek, D.E. Newby, E. D. Nicol, Coronary Artery Plaque Characteristics Associated With Adverse Outcomes in the SCOT-HEART Study, J Am Coll Cardiol 73 (3) (2019) 291–301.
[21] V. Mergen, T. Sartoretti, G. Cundari, M. Serifovic, K. Higashigaito, T. Allmendinger, B. Schmidt, T. Flohr, R. Manka, M. Eberhard, H. Alkadhi, The Importance of Temporal Resolution for Ultra-High-Resolution Coronary Angiography: Evidence From Photon-Counting Detector CT, Invest Radiol (2023).
[22] T.W. Holmes, Z. Yin, G.M. Stevens, S. Slavic, D.R. Okerlund, J.S. Maltz, A. Pourmorteza, Ultra-high-resolution spectral silicon-based photon-counting detector CT for coronary CT angiography: Initial results in a dynamic phantom, J Cardiovasc Comput Tomogr (2023).